Supplementary Information (SI) for Physical Chemistry Chemical Physics.
This journal is © the Owner Societies 2026

Supporting Information

Possible outcome of sunlight-promoted photoinductive reactive pathways for the degradation of environmental pollutants 8-nitrofluoranthene and 9-nitrophenanthrene

Bojana D. Ostojić[a,*], Branislav Stanković[b], Dragana S. Đorđević[a] and Peter Schwerdtfeger[c]

[a] *Center of Excellence in Environmental Chemistry and Engineering, Institute for Chemistry, Technology and Metallurgy, University of Belgrade, Njegoševa 12, Belgrade 11000, Serbia*

[b] *Centre of Excellence for Hydrogen and Renewable Energy, Vinča Institute of Nuclear Sciences-National Institute of the Republic of Serbia, University of Belgrade, Mike Petrovića Alasa 12-14, 11351 Vinča, Beograd, Serbia*

[c] *Centre for Theoretical Chemistry and Physics (CTCP), The New Zealand Institute for Advanced Study (NZIAS), Massey University, Auckland Campus, Private Bag 102904, North Shore City, 0745 Auckland, New Zealand*

* corresponding author

Contents

Computational details

Geometry optimizations for the selected singlet and triplet excited states of 9NPh and 8NFlu were performed using the complete-active-space self-consistent-field (CASSCF) method.[1,2] The geometries for the minimum energy points on the singlet–triplet seam of crossing were also obtained using the CASSCF method.[3] The active space for the CASSCF geometry optimizations of the excited singlet and triplet states of 9NPh as well as for the selected singlet-triplet minimum energy crossing points comprised of 10 orbitals. The chosen active space was selected to include the seven π orbitals which are admixture of the phenanthrene unit π orbitals and the π orbital of the nitro group, or are located mainly on the phenanthrene unit, one π orbital localized on the nitro group oxygens π_O, and two orbitals that involved lone pairs on the oxygen atoms of the nitro group (Figure S1). The restriction of the active space to less than ten orbitals lead to a poor description of the wave function at the CASSCF level. Extensive test calculations have been performed to explore the dependance of the geometries and energies along the reaction pathway on the active space. The active space for the energy profiles along the reaction pathway involved 12 orbitals for 9NPh. To highlight the relevance of the proper active space selection employed for the CASSCF (and subsequent CASPT2) calculations, the results obtained for the $(^3\pi_O\pi^*)_{min}$ state of 9NPh are presented in Figure S2. The CASSCF energies are plotted as the function of the size of the active space. The first active space (denoted as CAS no. 1 in Figure S2) tested involves 5 active orbitals (56a-60a). Inclusion of one more orbital (55a) in the active space (CAS no. 2) does not change substantially the CASSCF energy. A significant decrease of the CASSCF energy occurs when higher-lying orbitals (61a-63a) and one lower-lying orbital (54a) are included in the active space (CAS no. 3 in Figure S2). The CAS no. 5 as the most extensive active space was employed for the energy profiles along the reaction pathways of 9NPh.

The active space for the geometry optimizations of the singlet and triplet excited states of 8NFlu as well as for the selected singlet-triplet minimum energy crossing points comprised of six doubly occupied orbitals and five lowest unoccupied orbitals *i.e.* it was composed of 12 electrons distributed over 11 active orbitals (Figure S3). It consisted of 9 π orbitals located mainly on the fluoranthene unit, one π orbital localized on the nitro group, π_O, and one orbital that involved lone pairs of the oxygen atoms of the nitro group. We present in Figure S4 the dependance of the CASSCF energies on the selection of orbitals from the test calculations with different choices of active space for the energy profiles along the reaction pathways of 8NFlu. The results are obtained for the $(^3\pi_O\pi^*)_{min}$ state of 8NFlu. The minimal active space tested (CAS no. 1 in Fig. S4) consists of 6 orbitals (61a-66a). The results show that inclusion of the lower-lying orbital 59a mostly localized on the NO_2 group, as well as the higher-lying orbital 67a localized mainly on NO_2, qualitatively changes the results (CAS no. 3 in Fig. S4).

The state-averaged CASSCF (SA-CASSCF) calculations were performed including the selected singlet states and triplet states employing equal weights for all states. The geometry optimizations of the excited states and the geometries of the minimum energy points on the singlet–triplet crossing seem were performed using the Molpro program package.[4] The energy profiles along the pathways relevant for the photodegradation were calculated using the CASSCF method complemented by second-order perturbation theory (CASPT2) and the internally contracted multi-reference second-order perturbation theory code (RS2C)[5] as implemented in the program Molpro.[4]

The pathways from the minimum geometry of the lowest-lying triplet state of 8NFlu toward the dissociation products aryloxy radical (Ar-O˙) and NO˙ were set up by a geodesic interpolation.[6] With the help of the algorithm developed by Martinez *et al.* we have created segments joining the minimum geometry of the lowest-lying triplet and Ar-O˙ + NO˙. The number of segments corresponding to the intermediate geometries in the interpolation procedure between the initial and final geometries previously obtained through the geometry optimizations was set to 600.

In addition to the reaction path from 9NPh epoxide ring structure that leads to the NO˙ release (Fig. 13), we have also identified the transition state that leads to the isomerization of the epoxide to the corresponding oxepine (Fig. S5). It is well known that 9NPh as a nitro derivative of the angular polycyclic aromatic hydrocarbon exhibits some interesting characteristics. The most favoured position for epoxidation in 9NPh is the 9,10-position since the (9,10) double bond shows enhanced nucleophilic reactivity. The inspection of the result presented in Fig. S5 shows that product, the nitrite derivative of dibenz[b,d]oxepine, is stabilized by 4.4 kcal/mol compared to the reactant, epoxide ring structure. Therefore, the isomerization from the epoxide ring structure to the nitro derivative of dibenz*[b,d]*oxepine is thermodynamically feasible. However, the isomerization reaction is kinetically unfavoured since the system must surmount a barrier of ~2.5 eV, which is the energy difference between the epoxide ring structure and the transition state for that reaction. Therefore, the epoxide ring structure of 9NPh can be isomerized into the nitrite derivative of dibenz*[b,d]*oxepine but with higher energy compared to the direct transformation from epoxide ring into aryloxy radical and NO˙.

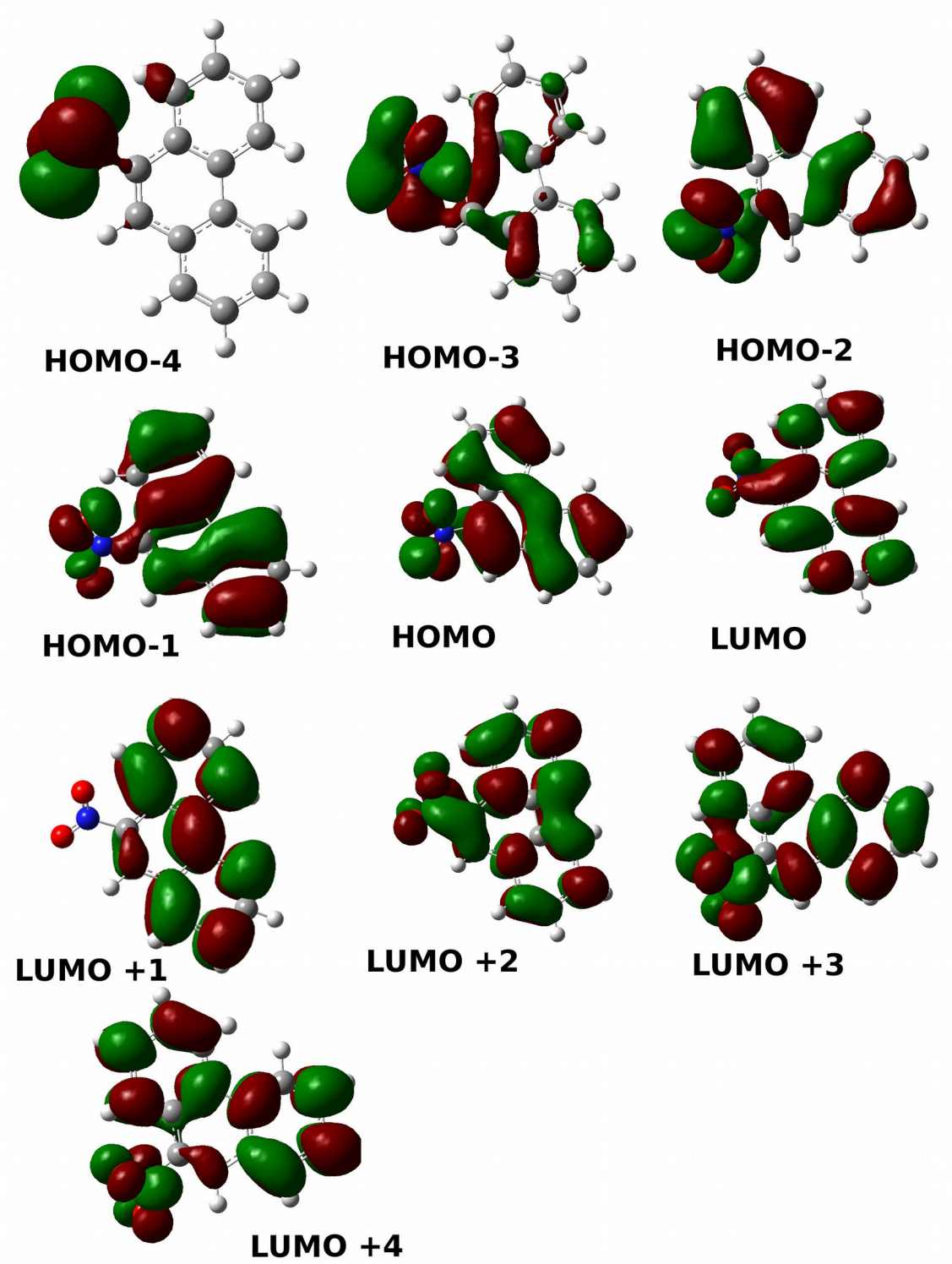

Fig. S1. Molecular orbitals included in the active space of the CASSCF optimization of the excited states of 9NPh.

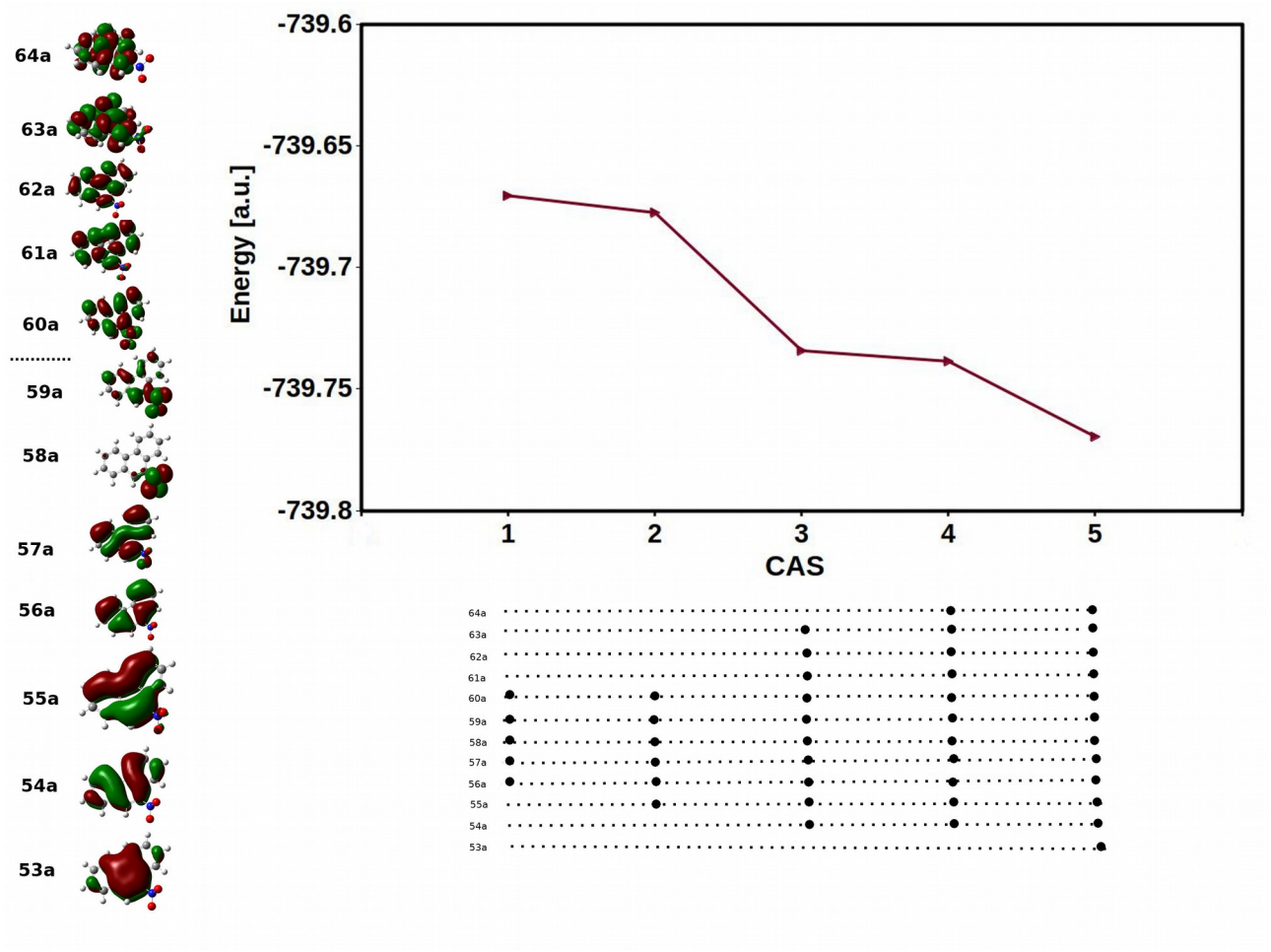

Fig. S2. The CASSCF orbitals determined at the equilibrium geometry of the $(^3\pi_O\pi^*)_{min}$ state of 9NPh (left panel). The CASSCF energy calculated at the equilibrium geometry of the $(^3\pi_O\pi^*)_{min}$ state of 9NPh as the function of the size of five active spaces. Dots below the graph denote orbitals included in the corresponding active space (right panel).

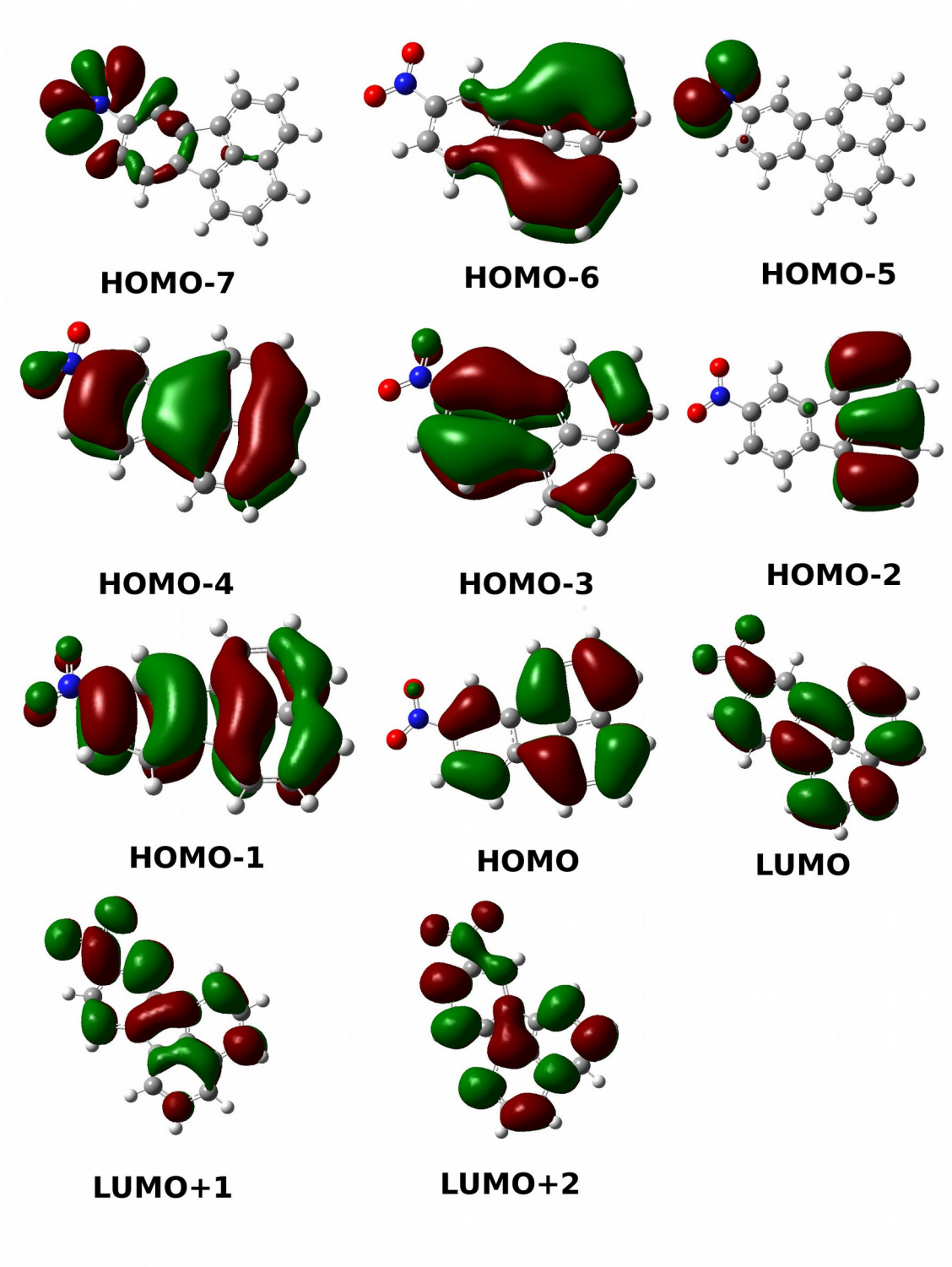

Fig. S3. Molecular orbitals included in the active space of the CASSCF optimization of the excited states of 8NFlu.

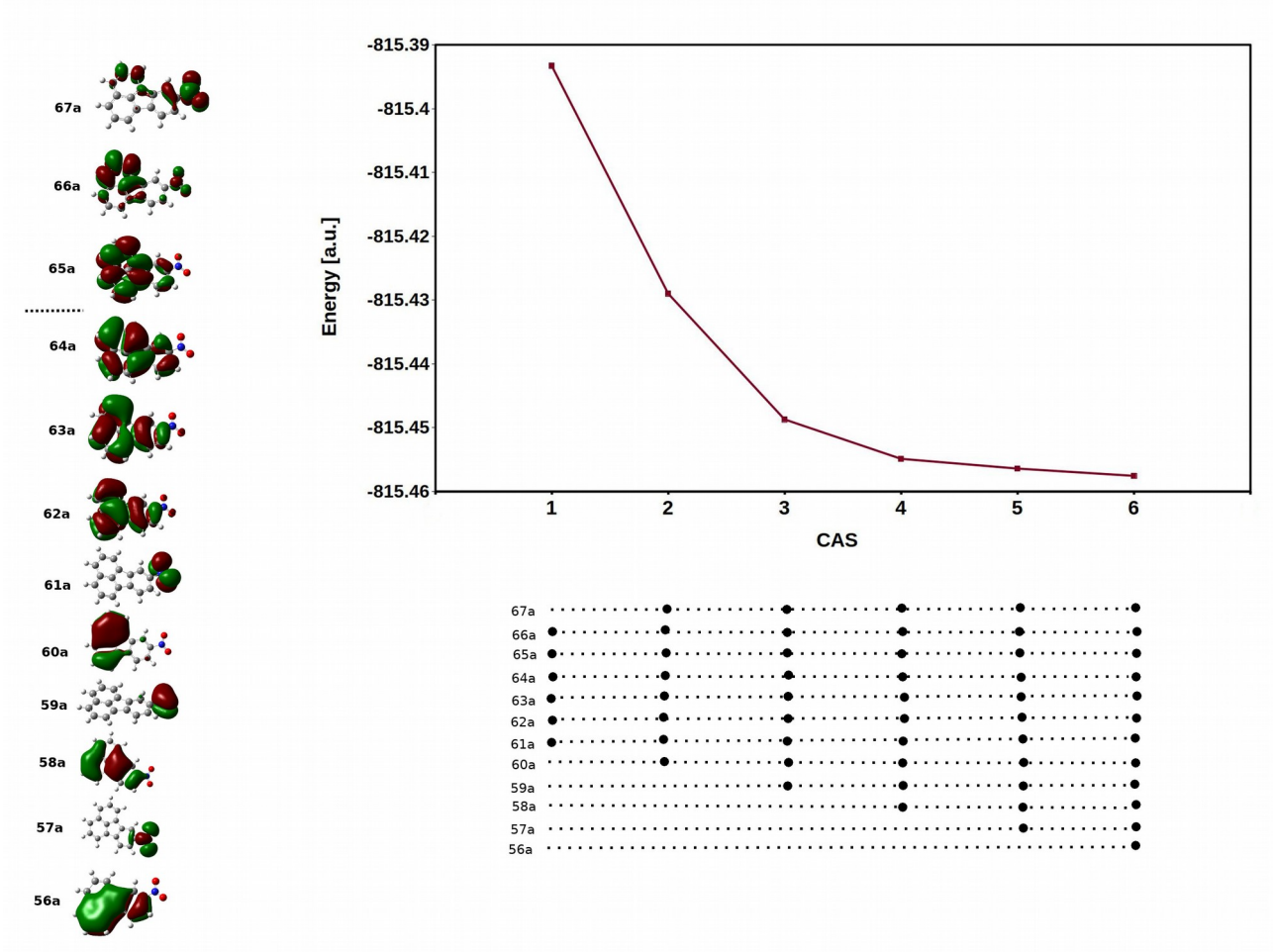

Fig. S4. The CASSCF orbitals determined at the equilibrium geometry of the $(^3\pi_O\pi^*)_{min}$ state of 8NFlu (left panel). The CASSCF energy calculated at the equilibrium geometry of the $(^3\pi_O\pi^*)_{min}$ state of 8NFlu as the function of the size of six active spaces. Dots below the graph denote orbitals included in the corresponding active space (right panel).

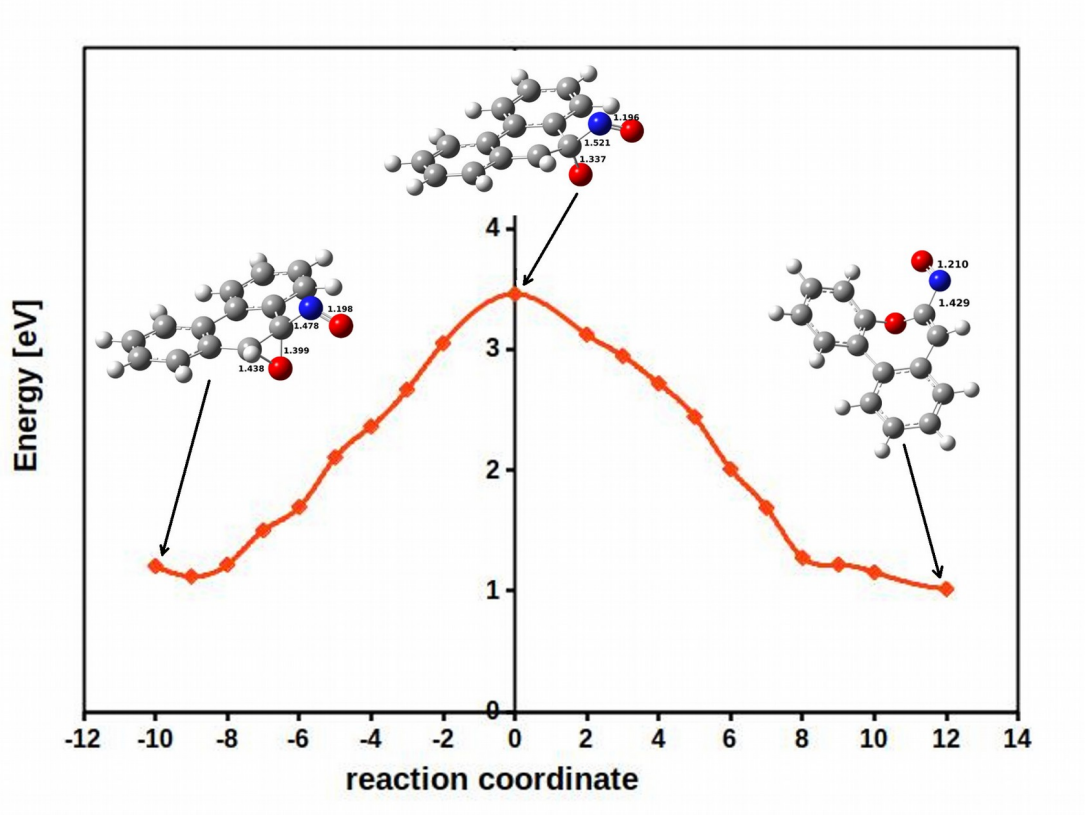

Fig. S5. Minimum energy pathway from the epoxide ring structure to the nitrite derivative of dibenz[*b,d*]oxepine on the singlet potential energy surface of 9NPh. The zero on the reaction coordinate axis refers to the transition state structure. The CASPT2/def2-TZVP single point energies are calculated at the IRC pathway obtained at M062X/6-311+G(d,p) level. The zero on the ordinate axis refers to the minimum energy of the ground state of 9NPh.

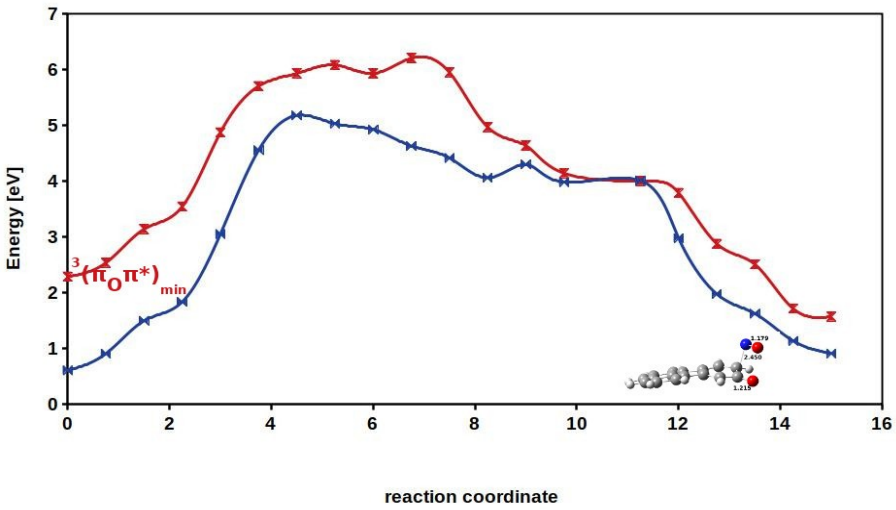

Fig. S6. Energy profile calculated at the CASPT2/def2-TZVP level along the geodesic interpolation pathway connecting the minimum geometry of the lowest-lying triplet state of 8NFlu, $(^3\pi_O\pi^*)_{min}$, with the Ar-O$^{\cdot}$ + NO$^{\cdot}$ dissociation products. The blue line refers to the singlet state while the red line is the triplet state. All energies are with respect to the minimum energy of the 8NFlu ground state.

References

1. H.-J. Werner, , P.J. Knowles, A second order multiconfiguration SCF procedure with optimum convergence Available to Purchase. J. Chem. Phys. 82 (1985) 5053–5063.

2. P. J. Knowles, H.-J. Werner, An efficient second-order MC SCF method for long configuration expansions. Chem. Phys. Lett. 115 (1987) 259-267.

3. T. Busch, A. Degli Esposti, H.-J. Werner, Analytical energy gradients for multiconfiguration self-consistent field wave functions with frozen core orbitals. J. Chem. Phys. 94 (1991) 6708-6715.

4. MOLPRO, version 2015.1, a package of *ab initio* programs, H.-J. Werner, P. J. Knowles, and others, see https://www.molpro.net.

5. P. Celani, H.-J. Werner, Multireference perturbation theory for large restricted and selected active space reference wave functions J. Chem. Phys. 112 (2000) 5546-5557.

6. X. Zhu, K. C. Thompson, and Todd J. Martínez, Geodesic interpolation for reaction pathways, J. Chem. Phys. 150 (2019) 164103.

7. M. J. Frisch, G. W. Trucks, H. B. Schlegel, G. E. Scuseria, M. A. Robb, J. R. Cheeseman, G. Scalmani, V. Barone, G. A. Petersson, H. Nakatsuji, X. Li, M. Caricato,

A. V. Marenich, J. Bloino, B. G. Janesko, R. Gomperts, B. Mennucci, H. P. Hratchian, J. V. Ortiz, A. F. Izmaylov, J. L. Sonnenberg, D. Williams-Young, F. Ding, F. Lipparini, F. Egidi, J. Goings, B. Peng, A. Petrone, T. Henderson, D. Ranasinghe, V. G. Zakrzewski, J. Gao, N. Rega, G. Zheng, W. Liang, M. Hada, M. Ehara, K. Toyota, R. Fukuda, J. Hasegawa, M. Ishida, T. Nakajima, Y. Honda, O. Kitao, H. Nakai, T. Vreven, K. Throssell, J. A. Montgomery, Jr., J. E. Peralta, F. Ogliaro, M. J. Bearpark, J. J. Heyd, E. N. Brothers, K. N. Kudin, V. N. Staroverov, T. A. Keith, R. Kobayashi, J. Normand, K. Raghavachari, A. P. Rendell, J. C. Burant, S. S. Iyengar, J. Tomasi, M. Cossi, J. M. Millam, M. Klene, C. Adamo, R. Cammi, J. W. Ochterski, R. L. Martin, K. Morokuma, O. Farkas, J. B. Foresman and D. J. Fox, Gaussian 16, Revision C.01, Gaussian, Inc., Wallingford CT, 2016.